Title
Modeling and Analysis of the Variability of the Water Cycle in the Upper Rio Grande Basin at High Resolution

Journal
Journal of Hydrometeorology, 8(4)

ISSN
1525-755X

Authors
Li, J
Gao, X
Sorooshian, S

Publication Date
2007-08-01

DOI
10.1175/jhm602.1

Modeling and Analysis of the Variability of the Water Cycle in the Upper Rio Grande Basin at High Resolution

J. LI, X. GAO, AND S. SOROOSHIAN

Center for Hydrometeorology and Remote Sensing, Department of Civil and Environmental Engineering, University of California, Irvine, Irvine, California

(Manuscript received 13 April 2006, in final form 8 December 2006)

ABSTRACT

Estimating the water budgets in a small-scale basin is a challenge, especially in the mountainous western United States, where the terrain is complex and observational data in the mountain areas are sparse. This manuscript reports on research that downscaled 5-yr (1999–2004) hydrometeorological fields over the upper Rio Grande basin from a 2.5° NCEP–NCAR reanalysis to a 4-km local scale using a regional climate model [fifth-generation Pennsylvania State University–National Center for Atmospheric Research Mesoscale Model (MM5), version 3]. The model can reproduce the terrain-related precipitation distribution—the trend of diurnal, seasonal, and interannual precipitation variability—although poor snow simulation caused it to overestimate precipitation and evapotranspiration in the cold season. The outcomes from the coupled model are also comparable to offline Variable Infiltration Capacity (VIC) and Land Data Assimilation System (LDAS)/Mosaic land surface simulations that are driven by observed and/or analyzed surface meteorological data.

1. Introduction

Investigating river basin water cycles in the western U.S. mountainous region poses great challenges for the hydrology community because the region's multiscale terrain leads to complex atmosphere–land surface interactions and makes it difficult to produce accurate observations. However, over the western United States, especially in the southwest semiarid region, the limited supply and increasing demand for water resources require accurate estimates of regional and local-scale hydrologic variability that result from interactions between climate and human influences. The upper Rio Grande basin is a typical case. The Rio Grande has its headwaters in the San Juan Mountains in Colorado, runs southward through New Mexico, continues through western Texas, and then becomes the border between Texas and Mexico, until it finally flows into the Gulf of Mexico. The upper Rio Grande is the stretch from the headwaters to Fort Quitman, western Texas, before it turns into the U.S.–Mexico border. The narrow, north–south stretching upper Rio Grande basin is bounded by the U.S. Continental Divide on the west and by the Sangre de Cristo Mountains on the east and covers an area of 92 000 km^2. The basin's elevation varies considerably, from over 4200 m at the highest elevation of the San Juan Mountains to less than 1200 m in El Paso, Texas. The basin's water resources include both surface water and groundwater. Seasonal precipitation, including the wintertime, large-scale, front snowfall, primarily over the San Juan Mountains, and the summertime, localized, monsoon-associated convective rainfall, is the main source for the river flow and groundwater recharge. The average annual precipitation varies from more than 130 cm at the high-elevation north to less than 15 cm in the low-elevation southern parts of the basin. Because the basin's population and economy have grown rapidly, currently the river gains water only above Santa Fe, New Mexico, and loses water farther south. The upper Rio Grande basin frequently confronts water shortages. Numerous "water rights" conflicts must be resolved in the courts, so the Rio Grande is sometimes called a "river of law" (http://www.ibwc.state.gov/wad/rioproj.htm). Clearly, competing uses of water resources may eventually deplete the groundwater, cause water quality to deteriorate, and require allocation of surface water (http://

Corresponding author address: Jialun Li, CHRS, Department of Civil and Environmental Engineering, University of California, Irvine, Irvine, CA 92697-2175.
E-mail: jialunl@uci.edu

DOI: 10.1175/JHM602.1

www.lanl.gov/chinawater/documents/wrriogrande.pdf). Therefore, there is a compelling need for atmospheric and hydrologic models that can accurately assess the basin's water budget components and their variability at space and time scales.

Many previous studies that include the upper Rio Grande basin have used the coupled atmosphere–land surface regional climate model (RCM) to analyze the hydroclimatic characteristics of the western mountainous region. These studies have addressed regional climate regimes (Giorgi and Bates 1989; Giorgi et al. 1993, 1994; Anderson et al. 2004; Xu et al. 2004; Kim and Lee 2003; Leung et al. 2003a), hydrologic cycles (Roads et al. 1994; Roads and Chen 2000; Leung et al. 2003b; Anderson and Kanamaru 2005), and precipitation distributions (Leung and Qian 2003; Liang et al. 2004). These studies have produced many important results that have improved our understanding of western U.S. hydroclimatology. Needless to say, they have also revealed some deficiencies in the models, chief among them are 1) the RCM's grid spatial resolution (usually greater than 30 km) was insufficient to represent atmosphere–land surface interactions over the western United States, which are induced by the complex terrain (as argued by Roads et al. 1994; Leung et al. 2003a,b; Anderson et al. 2004), and 2) many physical schemes in the RCM, in particular, the convective parameterization, cloud radiation, and land surface schemes, possess substantial errors (Gochis et al. 2003; Liang et al. 2004). In general, finer grid resolutions and more effective model physics are needed to improve RCM simulation.

From a hydrologic point of view, the relevance of the RCM numerical simulations depends to a large extent on the simulation's resolutions. Unfortunately, most current RCM grid resolutions, such as those adopted by the National Weather Service River Forecasting System (NWSRFS), are coarser than the requirements for river basin models. Arguably, high-resolution RCM studies that can capture the spatial variability of hydrologic/hydroclimatic variables, topography, and vegetation and soil characteristics are both desirable and necessary. Such studies will contribute to an improved understanding of water and energy budgets over small- to medium-sized river basins.

To improve our understanding of the hydrological cycle in the upper Rio Grande basin, this paper provides a 5-yr (1999–2004) assessment of the basin's hydroclimate using the fifth-generation Pennsylvania State University–National Center for Atmospheric Research (Penn State–NCAR) Mesoscale Model (MM5) at a very high grid resolution of 4 km. This paper's hypothesis is that a 4-km grid spacing can better resolve the complex terrain in the river basin and the surrounding regions and, more importantly, enable precipitation (rain and snow) production to be based more on the model cloud microphysics scheme than on the convective parameterization scheme. Cloud microphysics attempts to simulate the cloud's dynamical and thermodynamical processes explicitly and to eventually avoid the problems of convective parameterization schemes. The results observed in cloud microphysics can lead to many physical insights into the atmospheric system, even though they still include numerous uncertainties. This paper will focus on analyzing the basin's hydrological variables and their variability in the atmosphere–land surface system.

This paper's specific objectives are to 1) evaluate the results using very high spatial resolution simulations, 2) display the hydrological cycles of the atmosphere–land surface system over the upper Rio Grande basin and their variability at diurnal, seasonal, and interannual scales, and 3) identify the model deficiencies that are responsible for the major simulation errors.

2. Methodology

This manuscript addresses hydrological processes over the upper Rio Grande basin primarily using model output and some observational and analytic data. The model's configuration and performance are addressed as follows.

The study period is from June 1999 to September 2004. Four nested and two-way communication domains were used (see Fig. 1) for the downscaling. In the two-way communication between nested domains, not only do the results in the coarser domain affect the enclosed finer domain simulation, but the finer domain results also provide feedback to influence the coarse domain simulation. Domain 1 (D1), at a 108-km grid resolution, covers the whole United States, Mexico, southern Canada, Central America, and the surrounding oceans. Domain 2 (D2) covers the western United States and northern Mexico at a 36-km grid resolution. Domain 3 (D3) covers the southwestern United States, northern Mexico, and southern Utah and Colorado at a 12-km grid resolution. Finally, domain 4 (D4), at a 4-km grid resolution, covers the upper Rio Grande basin. Figure 2 shows the topography (kilometer), dominant vegetation types, and soil types in domain 4. The solid-line region in Fig. 2 represents the boundary of the upper Rio Grande basin that was used in this paper. Figure 2 indicates that high spatial resolution geophysical data resolve details of the topographical structure. The vegetation-type map indicates that shrubbery is the main land cover over the basin and that soil type is mostly sand loam.

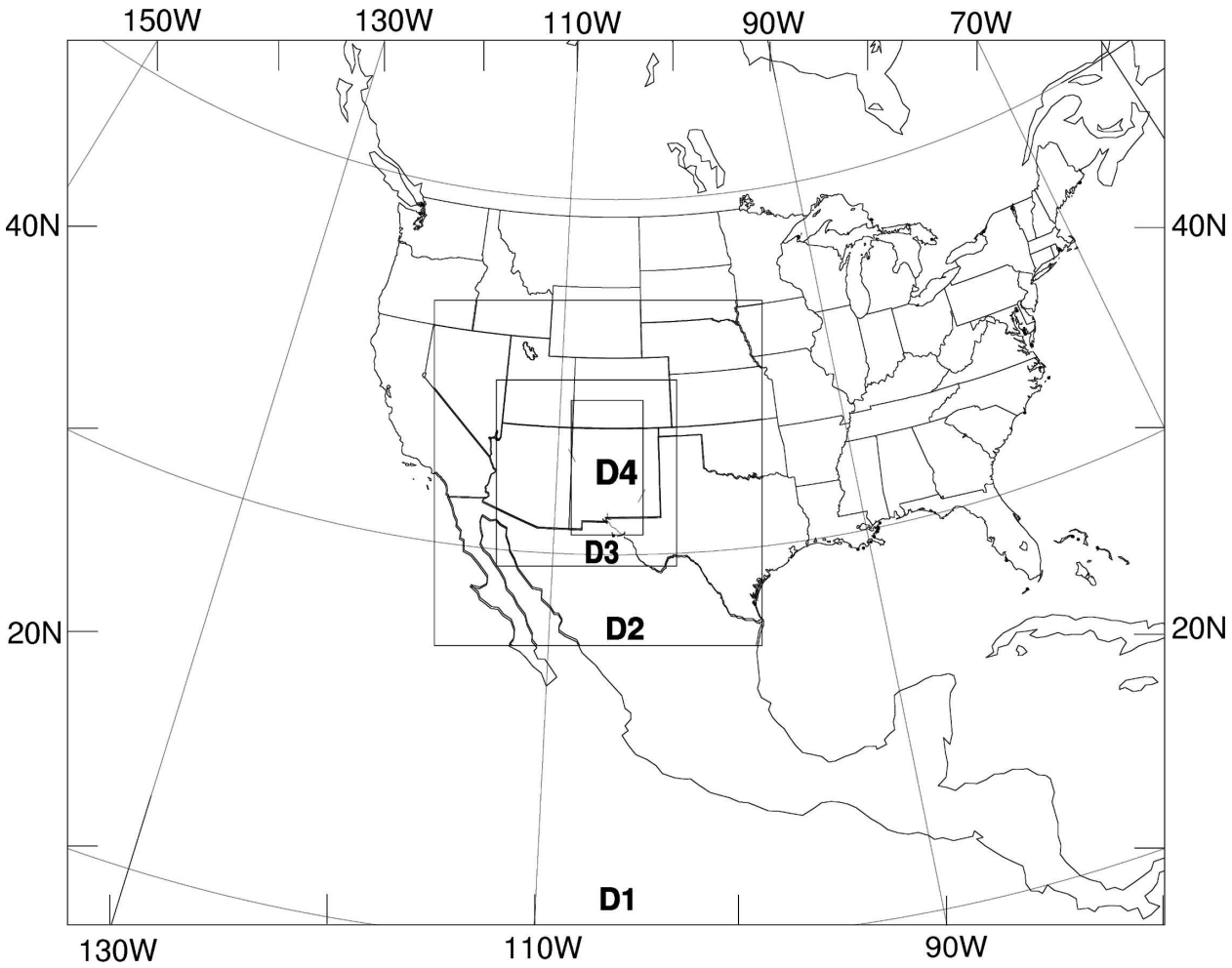

FIG. 1. Model domain setup; domain 1 (D1), domain 2 (D2), domain 3 (D3), and domain 4 (D4).

The Penn State–NCAR MM5 was employed for the integrated physical model because many researchers have used it to investigate land–atmospheric processes in the southwestern United States (Small 2001; Gochis et al. 2003; Xu et al. 2004; Li et al. 2005). Warner and Hsu (2000) have studied a severe storm that occurred in southern New Mexico and found that using the Grell (Grell 1993) convective parameterization scheme (CPS) in the coarse domain produced more realistic precipitation in the innermost finescale domain (also at a 4-km resolution) than the Kain–Fritch CPS did (Kain and Fritch 1990). Our sensitive tests of two summer seasons (summers of 1999 and 2003) showed that using the Grell CPS in domains 1, 2, and 3 led the model to generate more accurate rainfall distribution over low-elevation areas in domain 4 than the Kain–Fritch CPS did and that either the Kain–Fritch or Grell CPS caused the model to overestimate rainfall over the high-elevation areas in comparison with observations. Thus, this research used the Grell CPS in domains 1, 2, and 3. Other selected physically based schemes included the cloud radiation scheme (Dudhia 1989), the Medium-Range Forecast (MRF) boundary layer scheme (Hong and Pan 1996), and the Noah land surface model (Chen and Dudhia 2001).

National Centers for Environmental Prediction (NCEP) reanalysis data (at a 2.5° resolution) were used as the initial and boundary forcing data. Reynolds $1° \times 1°$ sea surface temperature (SST) data were used as the oceanic surface boundary forcing. The Reynolds SST is the only dataset archived in the study's time periods, although a preliminary study by our group showed that rainfall distribution and amount may be influenced by using different types of SST datasets in MM5 (Li et al. 2005).

In addition to testing physics processes to be used in the run, we also tested the soil moisture spinup issue using the month of July 1999. Liang et al. (2004) argued

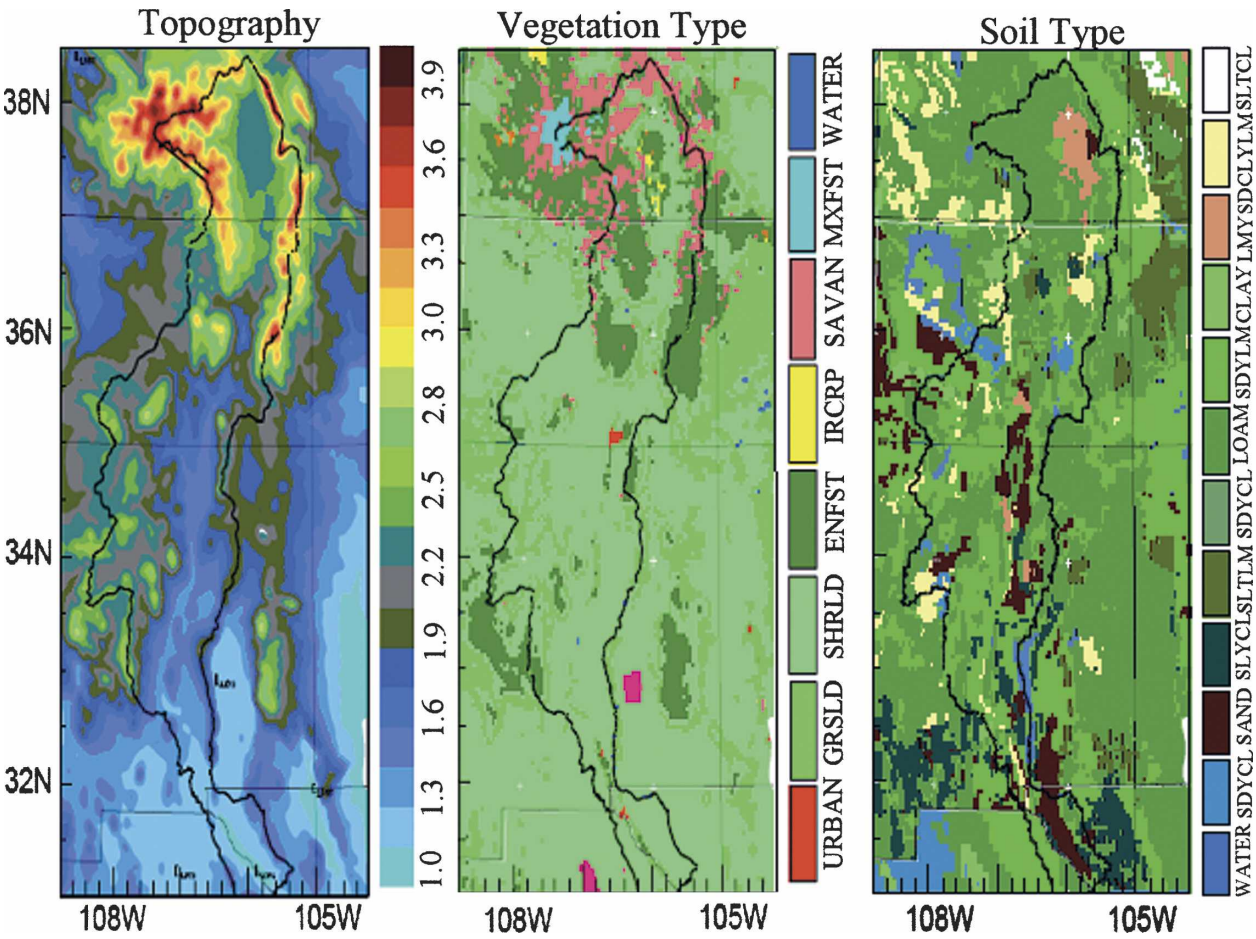

FIG. 2. The 4-km resolution model topography (km), dominant soil type, and dominant vegetation categories in domain 4. The circled solid line indicates the boundary of the upper Rio Grande used in this manuscript.

that 1 month of spinup is sufficient for their long-term (20 yr) runs. For the 1-month test runs, we examined soil moisture variations with no spinup and with 5-, 10-, 20-, and 30-day spinup. Figure 3 shows the daily soil moisture variations in the topsoil layer (10 cm) and the third soil layer (60 cm), which are averaged over domain 4. The results indicate that 1) during the first few days, the soil moisture at the top layer decreased quickly, 2) after about 1-week integration, the modeled topsoil moisture starting from different days converged closely, and 3) the third layer soil moisture variations were similar but maintained a drying trend. Xu et al. (2004) found that the soil moisture had a dry bias over the region when MM5/Oregon State University land surface model (OSU-LSM) was used. Based on this test, we set a 10-day spinup time period for each of four cold months (December, January, February, and March) and for each month in other times of the year. For example, when we ran the results for June 1999, the model started from 0000 UTC 22 May 1999, but the results from the first 10 days were discarded. When we ran the period starting from December 1999, the model actually started at 0000 UTC 21 November 1999.

3. Hydrologic equations

MM5 generated only certain basic atmospheric variables and land surface parameters. Other hydrometeorological variables, such as water vapor convergence and precipitable water, had to be calculated from the model output. This manuscript calculates these variables following the methods of Berbery and Ramusson (1999) and Roads et al. (1994). The budget equation for the vertically integrated atmospheric water is

$$\frac{\partial W}{\partial t} + \nabla \cdot Q = E - P. \tag{1}$$

The basin budget equation for the vertically integrated surface and subsurface water is

$$\frac{\partial S}{\partial t} = -E + P - R. \tag{2}$$

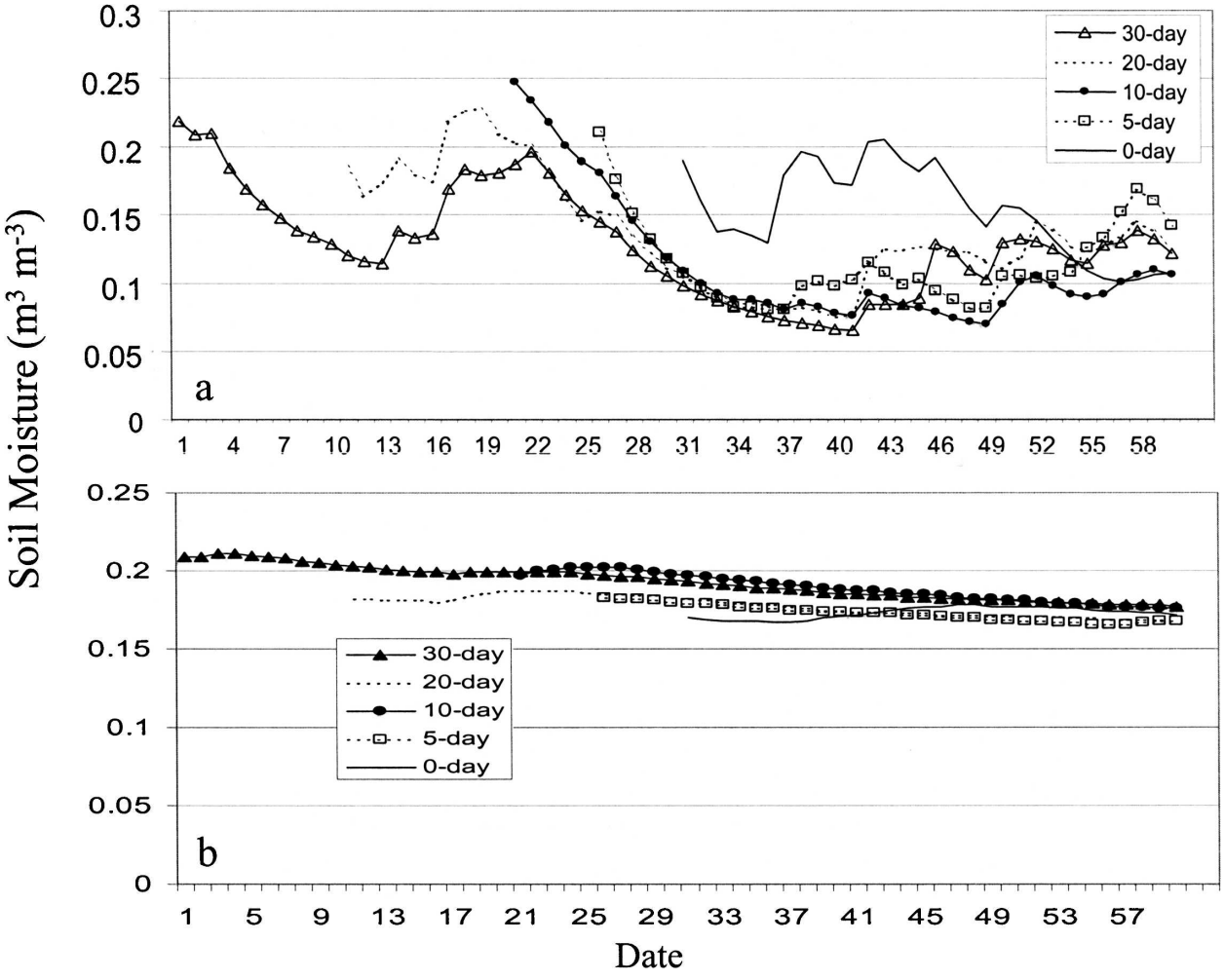

FIG. 3. Soil moisture daily variations in July 1999 for spinup tests over D4 for (a) the first layer (10 cm) and (b) the third layer (60 cm).

Here, W, Q, E, P, S, and R stand for precipitable water [Eq. (3)], integrated horizontal water vapor fluxes [Eq. (4)], evapotranspiration, precipitation, land surface water storage (including liquid and solid), and surface runoff or streamflow, respectively:

$$W = \frac{1}{g}\int_{P_t}^{P_s} q\, dp \quad \text{and} \tag{3}$$

$$Q = \frac{1}{g}\int_{P_t}^{P_s} q\mathbf{v}\, dp, \tag{4}$$

where P_t and P_s are the atmospheric pressure at the surface and top layer, respectively.

Recycling ratio (r), used in subsequent analysis, is defined according to Zangvil et al. (2004):

$$r = \frac{E}{E + C}, \tag{5}$$

where $C = -\nabla \cdot Q$ is the net water vapor inflow to the atmospheric column (i.e., convergence).

4. Evaluation of model results

The model simulation's performance was evaluated using the following observation and analysis data: 1) 25-km and daily precipitation analysis data from the National Weather Service (ftp://ftp.cpc.ncep.noaa.gov/precip/wd52ws/us_daily/); 2) stage-IV multisource (radar mixing with gauge) 4 km × 4 km, hourly precipitation data; 3) North American Regional Reanalysis (NARR) data (http://dss.ucar.edu/datasets/ds609.2) with 3-hourly and 32-km resolutions; 4) snowpack telemetry (SNOTEL) precipitation and snow water equivalent (SWE) measurements (http://www.wcc.nrcs.usda.gov/snotel/); 5) offline Variable Infiltration Capacity (VIC) model output at 0.125° spatial resolution (Maurer et al. 2002); and 6) offline Land Data Assimi-

lation System (LDAS)/Mosaic model 12-km output. The offline land surface models were driven by observed and analyzed surface meteorological data and therefore were expected to produce more realistic land surface hydrological data than the outcomes of the coupled model. The review paper of Mitchell et al. (2004) addressed the main features of the three land surface models, Noah, VIC, and Mosaic, and compared the model results during 1996–99, which indicated "substantial intermodel differences in surface evaporation, soil moisture storage, snowpack, and skin temperature."

Figure 4a compares the seasonal mean precipitation distributions between the NCEP gridded gauge data (25 km) and the model results (4 km) in domain 4 for the period from June 1999 to September 2004. The model reproduced the seasonal precipitation patterns shown in the observations but amplified precipitation intensity, particularly over the mountain areas, which is a common feature of downscaling using regional climate models over mountainous regions (Leung and Qian 2003; Leung et al. 2003b). In addition, in referring to the domain 4 topography (Fig. 2), the modeled high-resolution precipitation showed remarkable orographic features while the NCEP gauge data did not. As is well known, this is partly because the NCEP gauge data lack a sufficiently dense observation network over the mountains, resulting in a lack of coarse resolution and possible underestimation of precipitation. In summary, the model's precipitation feature indicated that high-resolution simulation was able to accurately represent the terrain-triggered precipitation mechanism.

Besides the orographic precipitation feature, strong rainfall diurnal variability over the upper Rio Grande basin during the monsoon season has been observed for a long time (e.g., Bowen 1996). Figure 4b shows the domain 4 rainfall diurnal cycle based on two sources: the hourly stage-IV (mixed gauge and radar) precipitation data and the model simulations during the monsoon seasons (June, July, August, and September) of 2002, 2003, and 2004. These 3-yr data were used because stage IV has only been available since January 2002. Both the observed and modeled results indicate that the rainfall in the region occurs mainly from late morning to midnight and there is no significant rainfall during the other hours of the day. The model reproduced the trend of precipitation diurnal variability, but in comparison with the stage-IV diurnal pattern, the modeled rainfall diurnal peak has a lower intensity (MM5: 0.12 mm h^{-1} versus stage IV: 0.15 mm h^{-1}) and a 4-h lag (0000 versus 0400 UTC). Anderson and Kanamaru (2005), using the global spectral model/regional spectral model (GSM/RSM) at a 25-km resolution, simulated five continuous summer seasons (July–September) to study the atmospheric hydrologic diurnal cycle over the southwestern United States. Their results for 6-h rainfall (their Fig. 2) show that the rainfall diurnal peak is about 0.08 mm h^{-1} during the 1800–0000 UTC time period. Gochis et al. (2003), using MM5 at a 30-km resolution, compared the impacts of different CPSs on monsoon rainfall diurnal variability over the Rio Bravo (i.e., the whole Rio Grande basin) and found that the Grell CPS shows that rainfall diurnal variation is extremely weak, with a peak value of 0.02 mm h^{-1}, while with the Kain–Fritch CPS, the rainfall diurnal peak increases to 0.12 mm h^{-1} and occurs at 2100 UTC (their Table 3 and Fig. 6). Compared with these previous studies, the MM5 4-km simulation is notably improved because the topographic representation is better than that of coarse resolution and the cloud microphysics scheme permits greater accuracy. The inaccurate diurnal rainfall variability (intensity and timing of the peak rainfall) may reflect a major limitation of model-generated precipitation in hydrologic applications, especially for flash flood forecasting.

Figure 5a shows the 1999–2004 monthly time series of mean precipitation over the basin based on the model simulation, NCEP 0.25° gridded gauge data, and VIC forcing precipitation (labeled "VIC-P" in the figure), which was interpolated to the VIC grid from the National Oceanic and Atmospheric Administration/National Climatic Data Center/Cooperative Observer Network (NOAA/NCDC/COOP) hourly gauge data (refer to Maurer et al. 2002). This figure shows that the modeled precipitation closely reflects the observed monthly precipitation variations. However, the two gauge datasets differ greatly, sometimes as much as 20 mm $month^{-1}$. The mean precipitation of the entire simulation period was 1.13 mm day^{-1} for the MM5 simulation, 0.965 mm day^{-1} for the NCEP gridded gauge data, and 1.01 mm day^{-1} for the VIC forcing precipitation (VIC-P hereafter). The MM5 model overestimated precipitation by 17% in comparison to the NCEP gridded gauge data and by 12% in comparison to the VIC gauge data. However, these overestimations may be an advantage for the model, given that sparse gauge observation network could mean that the network was insufficient to capture the relatively high intensive and frequent precipitation over the mountains.

Figure 5b compares the time series of precipitable water (instantaneous, in mm or $kg^2\ m^{-2}$) between the NARR reanalysis data (modeling with frequent observational data assimilations) and the MM5 4-km results over the basin. The MM5 model accurately reproduced the precipitable water variations.

Figure 5c is the time series of mean evapotranspira-

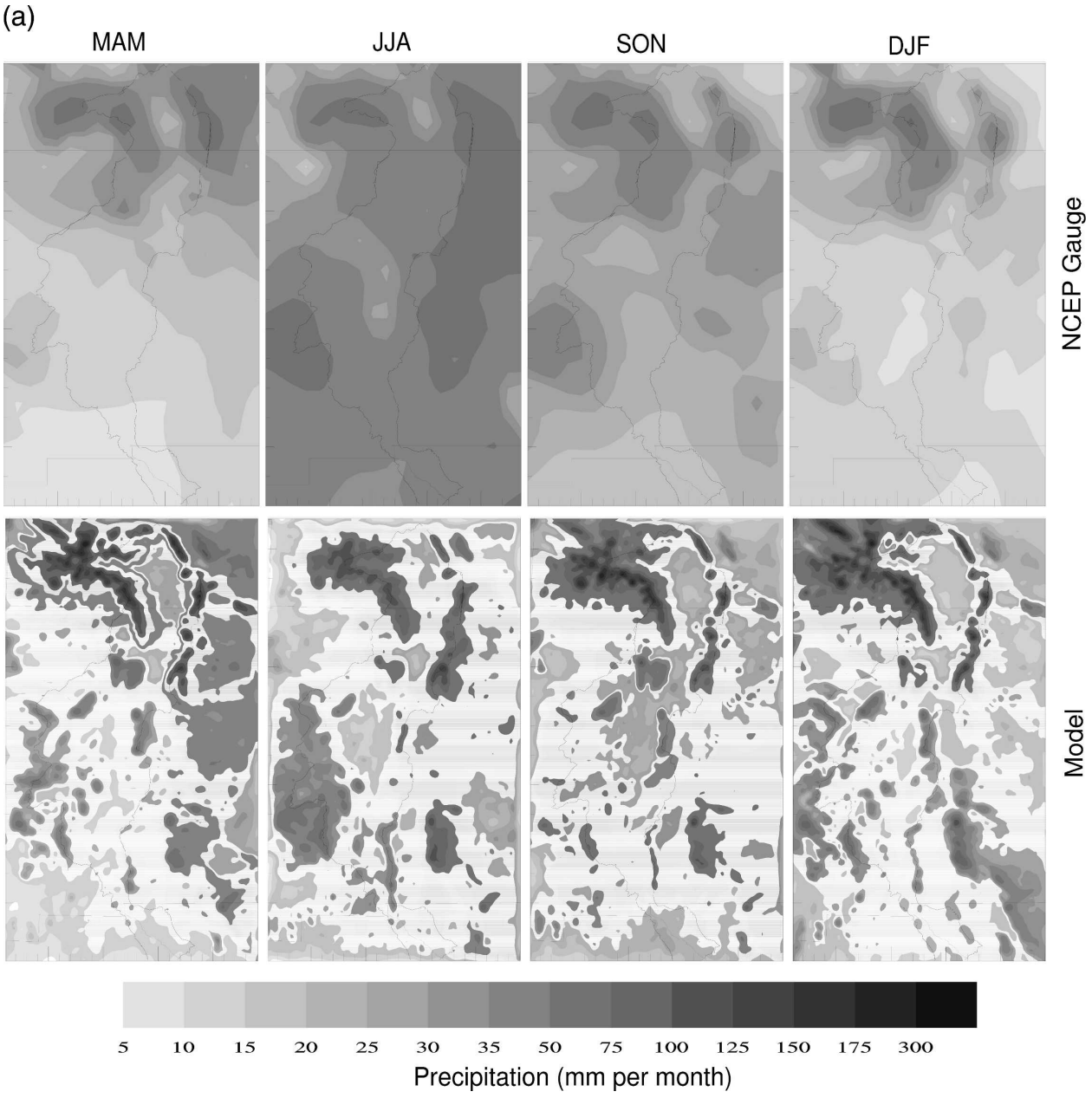

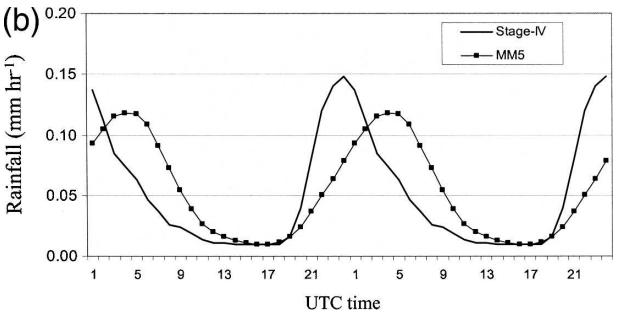

FIG. 4. (a) Mean precipitation comparison between NCEP gridded gauge data (25-km resolution) and MM5 model results in different seasons: spring [March–May (MAM)], summer [June–August (JJA)], fall [September–November (SON)], and winter [December–February (DJF)]. (b) Grid mean rainfall diurnal cycle comparison between MM5 results and stage-IV data over the basin. The grid mean was averaged as the gridpoint rainfall within the circled solid line in Fig. 2. The basin in D4 includes a total of about 6980 grid cells. The stage-IV data were first averaged hourly in the stage-IV domain and then interpolated linearly into D4. The data were from 2002 to 2004 because no stage-IV data were available before January 2002.

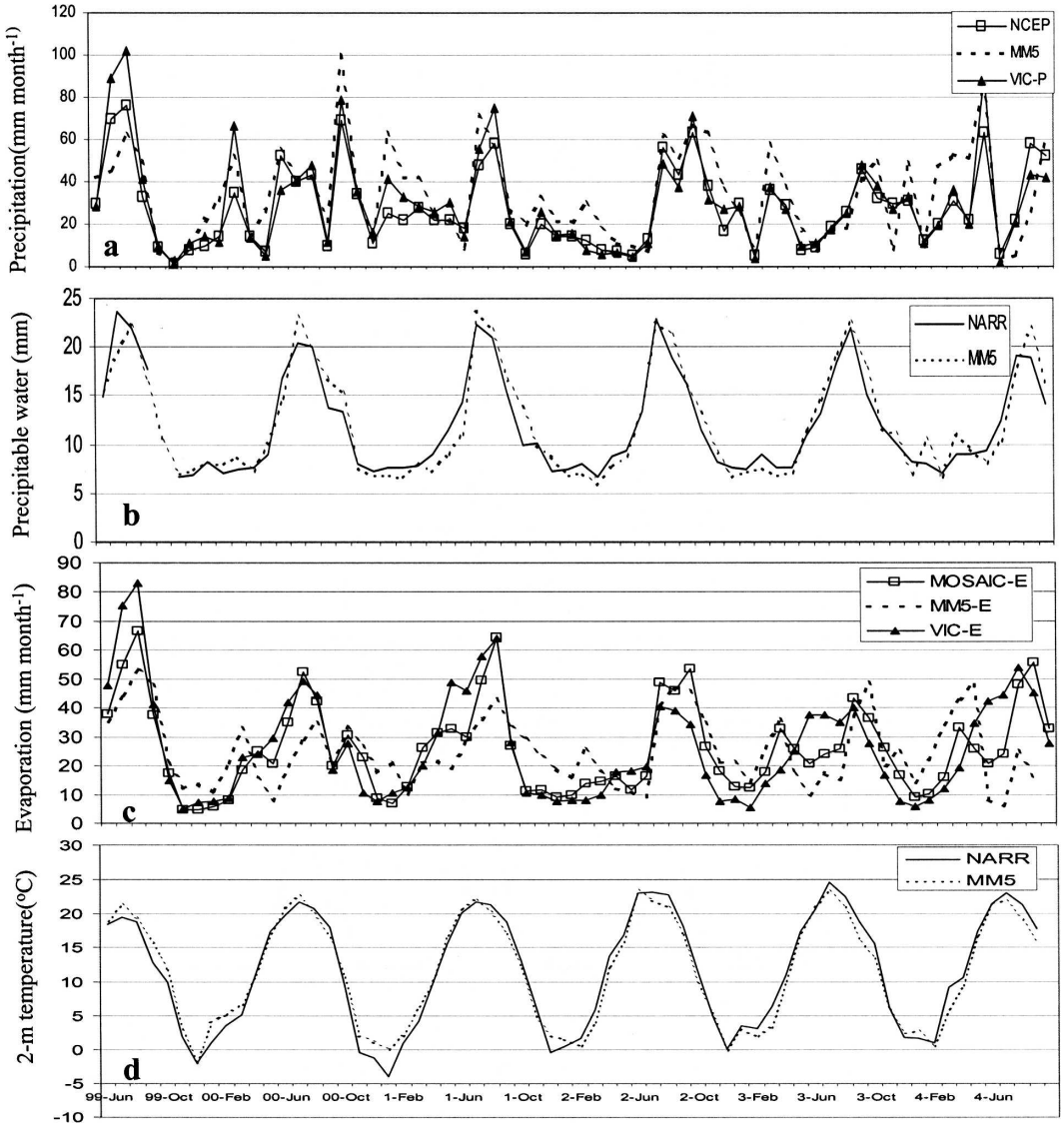

FIG. 5. Time series of (a) precipitation (mm month^{-1}), (b) precipitable water (instantaneous, mm), (c) evaporation (mm month^{-1}), and (d) 2-m air temperature (°C). NCEP stands for NCEP gauge 0.25° daily data, which include a total of about 247 grids within the basin. NARR represents NARR analysis data, which include about 150 grids within the basin. Mosaic indicates LDAS/MOSAIC data, which include about 840 grids in the basin. VIC indicates VIC model output. Note that VIC-P indicates VIC precipitation forcing data, which are interpolated from NOAA/NCDC/COOP gauge data the same as in the following figures. MM5 indicates the results from MM5 output, which includes about 6980 grids within the basin. The boundary of the upper Rio Grande basin is shown in Fig. 2.

tion (E, mm month^{-1}) from the MM5 simulation (MM5-E), offline Mosaic model output (Mosaic-E), and offline VIC model output (VIC-E). The coupled MM5 model reproduced the trend of evapotranspiration variations shown in the Mosiac and VIC time series, which were driven by the observed and analyzed surface meteorological data. The MM5 consistently overestimated modeled E in cold seasons (October to February) and underestimated it in warm seasons. The mean of E for the whole simulation period was 0.93 mm day^{-1} for the MM5 simulation, 0.78 mm day^{-1} for the Mosiac output, and 0.89 mm day^{-1} for the VIC output, which amounts to approximately a 19% (5%) difference per day between the MM5 and Mosaic (VIC) results.

Figure 5d shows the time series of 2-m temperature from the MM5 output and NARR reanalysis data. The model showed a relatively large positive bias of surface

air temperature in the cold seasons of 1999/2000 and 2000/01, which is related to the model snowpack simulations that will be addressed later.

The following section analyzes hydrologic processes over the upper Rio Grande basin to determine whether high-resolution MM5 simulation can provide additional useful hydrological information for the river basin that will fill in the sparse observational data we can obtain for the mountainous region.

5. Hydrologic results

a. Modeled climatology

Figure 6 presents the 5-yr mean climatology of water cycle components over the upper Rio Grande basin as obtained from the MM5 (top row), offline VIC (middle row), and Mosiac (bottom row) results. These components include precipitation (P), evapotranspiration (E), evaporation minus precipitation ($E - P$), time derivative of land surface water storage (S_t), and grid surface runoff (R). The runoff unit is in millimeters per month, while the units of the other variables are in millimeters per day. To avoid the figure being too busy, the atmospheric moisture flux convergence (C) and time derivative of precipitable water (W_t) are not plotted but will be discussed in the text. Note that the precipitation of Mosaic (Mosaic-P hereafter) was interpolated to the Mosaic grid point from the merged products of NCEP daily 0.25° gridded gauge precipitation and stage-II hourly 4-km observation precipitation (Cosgrove et al. 2003). The following patterns are observed in Fig. 6:

1) The precipitation maps (the first column) from the MM5 simulation and the VIC gauge forcing data were similar except that the MM5 precipitation amounts were larger over the basin's headwater area and over certain isolated mountains/hills in central New Mexico. The precipitation distribution from the Mosiac gauge forcing data differed slightly from that of the VIC forcing data in pattern and amount.
2) The evapotranspiration distributions (the second column) from the MM5 and VIC model outputs also were similar and were highly correlated to their precipitation distributions. Over the valley in the basin's headwater area, E from the MM5 output was larger than that from the VIC output, while E decreased slightly at the valley in the southern part of the basin. In comparing the geophysical maps of Fig. 2 with Fig. 6, Fig. 6 shows that the E pattern produced by MM5 in domain 4 was related to the distribution of vegetation types over the high-latitude area (especially the mountains) and to the soil types over the low-latitude area (especially the valleys). In contrast to the MM5 and VIC model results, the Mosaic model's simulation of the spatial distribution of evaporation showed relatively smooth variations over the basin.
3) The three models' maps of the difference of E minus P ($E - P$, the fourth column) show some interesting features for hydrological analysis at local scales. The MM5 $E - P$ map showed an amplified variation pattern in comparison with those from the VIC and Mosaic outputs. Although all three models indicated P was greater than E over most of the basin, over certain isolated valleys located along the river from north to south (dashed line circles in Fig. 6) the MM5-predicted E was greater than P, the VIC showed E was less than P but with differences that were much smaller than the values for the surrounding areas, and, similarly, the Mosaic showed E over the valley areas was generally slightly less than P, though in a few spots E was greater than P. Because the precipitable water time derivative was relatively small (<0.1 mm day^{-1}) in comparison with other atmospheric hydrologic components in Eq. (1), $\nabla \cdot Q \approx E - P$. In other words, areas with $E < P$ possess water vapor convergence and vice versa. Based on the climatological pattern exposed by the high-resolution MM5 simulation, those valley areas experienced atmospheric water divergence for the five years that were studied.
4) All three models predicted that the mean grid runoff (the fifth column) would be relatively small and were realistic for the semiarid region. However, the VIC model generated a larger runoff than the MM5 did, although the gauge-based VIC precipitation was less than the precipitation in the MM5 model. The runoff from Mosaic was the greatest over the uppermost (headwater) area and the least over the southernmost area of the basin.
5) Neglecting the runoff term in Eq. (2) allows us to figure the time derivative of the land surface water storage $S_t \approx -E + P$. The patterns of $E - P$ and S_t in Fig. 6 are inversely correlated, indicating that in areas with atmospheric water vapor divergence ($E > P$) S_t decreases, and in areas with atmospheric convergence ($E < P$) S_t increases. Figure 6 indicates that S_t from the VIC and Mosaic systems slightly increased for the 5-yr mean (i.e., $S_t > 0$), while the S_t from MM5 clearly shows that it decreased at some specific areas (see the solid circles at the last column in Fig. 6) and increased over the other areas. The mean S_t over the basin was also greater than 0 in the MM5 system. The possible reason for S_t variation in

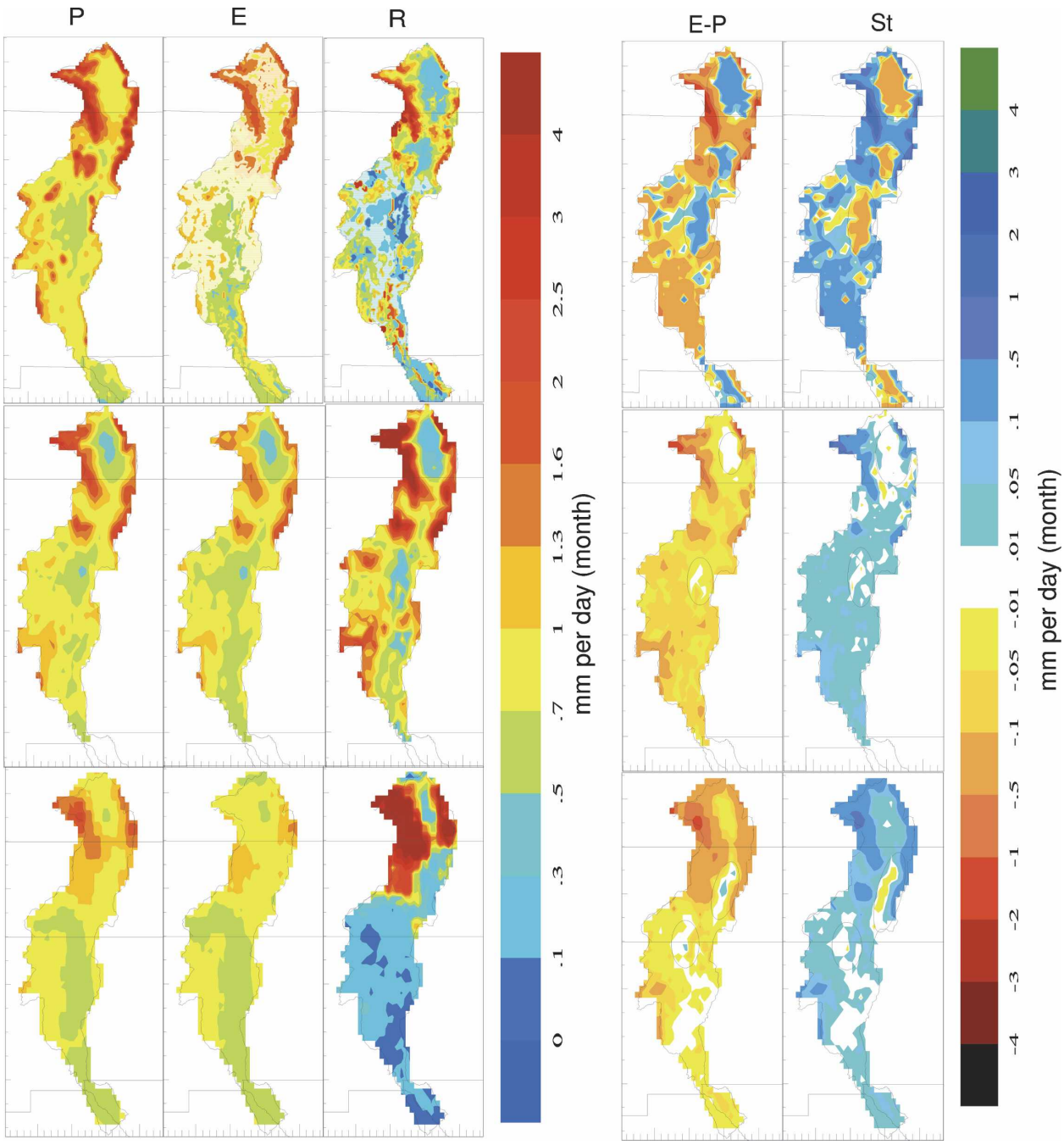

FIG. 6. Model hydroclimatology from (top) MM5, (middle) VIC, and (bottom) Mosaic for the upper Rio Grande basin during the simulation period [mm day^{-1}, except surface grid runoff (mm month^{-1})]. Here P, E, S_t, and R stand for precipitation, evaporation, time derivative of land surface storage, and grid runoff, respectively. The circles show the areas that $E - P > 0$ and $S_t < 0$.

MM5 will be addressed later. Based on the climatological patterns exposed by the high-resolution MM5 simulation, those valley areas ($E > P$) stayed dry in the 5-yr study period and might need outside water (pumping from the river or groundwater) to stop the natural loss of water storage.

The 5-yr mean of hydrological components over the upper Rio Grande basin was $P \sim 1.13$ mm day^{-1}, $E \sim 0.93$ mm day^{-1}, $C \sim 0.26$ mm day^{-1}, $W_t \sim 0.04$ mm day^{-1}, and $R \sim 0.024$ mm day^{-1}. To understand the physical conditions that were represented by the relationships among these numbers, the recycling ratio (r)

was estimated. Equation (5) gives the mean recycling ratio over the basin, $r = 0.78$. This recycling ratio indicates that approximately 78% of the precipitation came from the recycling moisture via E from the land surface, and approximately 22% came from the atmospheric moisture via advection convergence. Using five years' worth of summer season simulation data (July 1998–September 2002), Anderson et al. (2004) estimated that the recycling ratios for individual grid points over the southwestern United States ranged from 0.7 to 0.9. Compared to the results of Anderson et al., the current study's estimated annual recycling ratio is reasonable because it includes the relatively weak evaporation time period in cold seasons.

Figure 7 illustrates how P, E, and C vary with elevation over the upper Rio Grande basin in the three model simulations. Because W_t was unavailable in offline cases, C was estimated by $P - E$ (assuming that W_t is negligible) in the VIC and Mosaic simulations. The P, E, C, and elevation data from the three models were first interpolated onto the 12-km grid cells of domain 3 and then plotted for comparison. Generally, P, E, and C all increased with terrain elevation. The increase was faster in MM5 than in VIC and Mosaic when the elevation was higher than 2 km. Figure 7 also indicates the following features:

1) In a comparison of data from different models, the curves show that when precipitation increased with elevation the data were the same at the low-elevation range (<2.5 km) but diverged at the high-elevation range (>2.5 km). MM5 precipitation increased at the fastest rate, possibly because the observation networks were sparse and the MM5 overestimated precipitation over the mountains. Precipitation measurements (filled circles) at 22 SNOTEL stations were also plotted in Fig. 7. Although the SNOTEL data were characterized by high scattering, they indicated that the MM5 precipitation reflected the observed trend reasonably well, while the gauge-based VIC and Mosaic precipitation data underestimated the increases in precipitation rate with elevation.
2) Similar to precipitation, the three models' E curves also matched each other at low elevations but diverged at elevations higher than 2.5 km. The E curves from VIC and Mosaic flattened with elevations greater than 3 km, while the E curve from MM5 continued rising with elevation.
3) The convergence shown by the different models at low elevations (<2.5 km) was very small, but it increased when the elevation increased and finally reached the same magnitude as evaporation at elevations greater than 3 km.

Figures 6 and 7 indicate that in the upper Rio Grande basin, E is the major hydrologic component that provides moisture for P, especially over low-elevation areas. As elevation increases, C contributes more and more moisture to P. These results indicate that as one would expect, the hydrologic features of the upper Rio Grande basin are highly related to variability in topography in specific regions. The high-resolution model has shown the capability to reproduce many local-scale hydrologic features within the basin and thus has potential usefulness as a tool for water resource applications.

b. *Interannual variability*

Figure 8a depicts the interannual variation of the modeled mean precipitation (P: solid), evaporation (E: dashed), convergence (C: solid with square), time derivative of precipitable water (W_t: solid with triangle), time derivative of land surface water storage (S_t: solid with plus), and surface grid runoff (R: dashed with cross) during the five water years (a water year is defined as running from October to the following September). The variations in C and S_t corresponded highly to that of P, which can be understood through Eqs. (1) and (2) if we consider the fact that values for W_t and R are small in comparison with P, C, E, and S_t. Therefore, the relationship between these variables can be expressed as $-C \approx E - P$ (or $P = C + E$), $S_t \approx P - E$, and $S_t \approx C$. These relationships indicate that an increase in E will increase P, but this "recycling" portion of P will not change S_t: only the portion of P that derives from C—the moisture transported from outside into the system—will change S_t, the system's major water storage time derivative. Kanamitsu and Mo (2003) also emphasized the importance, in comparison with soil moisture and/or evaporation, of how the atmospheric moisture transported from outside into the southwestern United States in turn affects local precipitation. Numerous studies indicate that the moisture in the southwestern United States comes mainly from the Gulf of California, the tropical and eastern Pacific, and the Gulf of Mexico (Anderson et al. 2004; Kanamitsu and Mo 2003; Schmitz and Mullen 1996; Gochis et al. 2003).

Figure 8b compares the annual P and E from the three models for the five-water-year period. The interannual precipitation variations between the MM5 simulation and the VIC and Mosaic forcing data were similar except that the MM5 model amplified the precipitation amount, implying that MM5 estimates are consistently greater than the gauge-based data.

The evapotranspiration (E) did not exactly follow the interannual variability of the precipitation, conver-

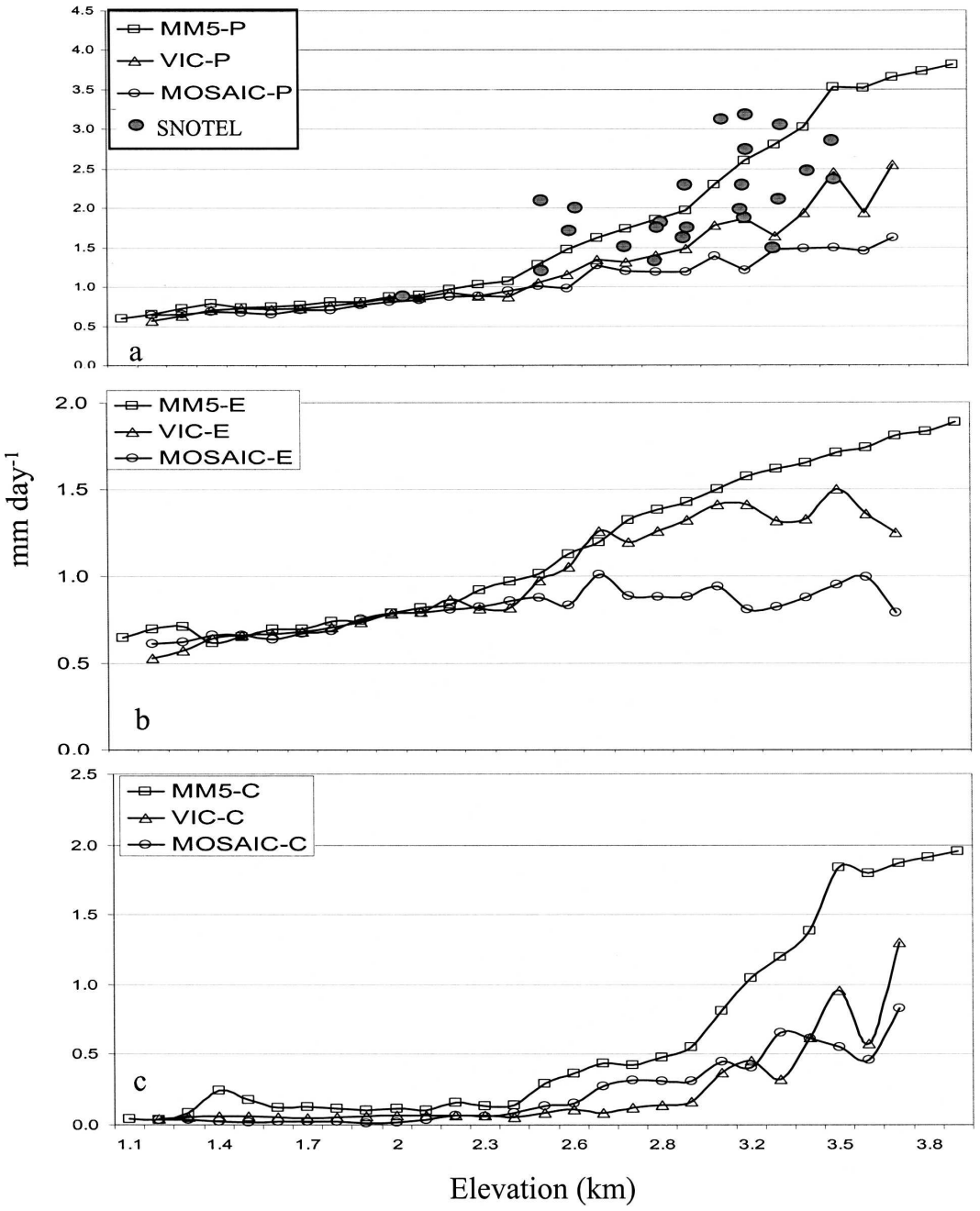

FIG. 7. The relationship between hydrologic components and elevation (km) over the upper Rio Grande basin: (a) precipitation, (b) evaporation, and (c) convergence. MM5, VIC, and Mosaic indicate the variables from MM5, VIC, and Mosaic model output. VIC-C was estimated using $P - E$, as was Mosaic. The filled circles represent precipitation, including 22 SNOTEL stations and two routine meteorological observation stations: Taos (2 km) and Gulf Greek Pass (3.2 km).

gence, or surface storage, partly because of the effects of soil and vegetation types, which include complex processes: after precipitation infiltrated in soil, soil properties will control how much water could be stored and how fast the water in the pore will be drained. Vegetation root depth will determine how deep the plants can extract water from the soil, and the leaf area index (LAI) will have an effect on the amount of E water to the canopy. In current land surface models (e.g., the Noah in MM5), the properties of soil and vegetation are preset and not changed with the climate variations.

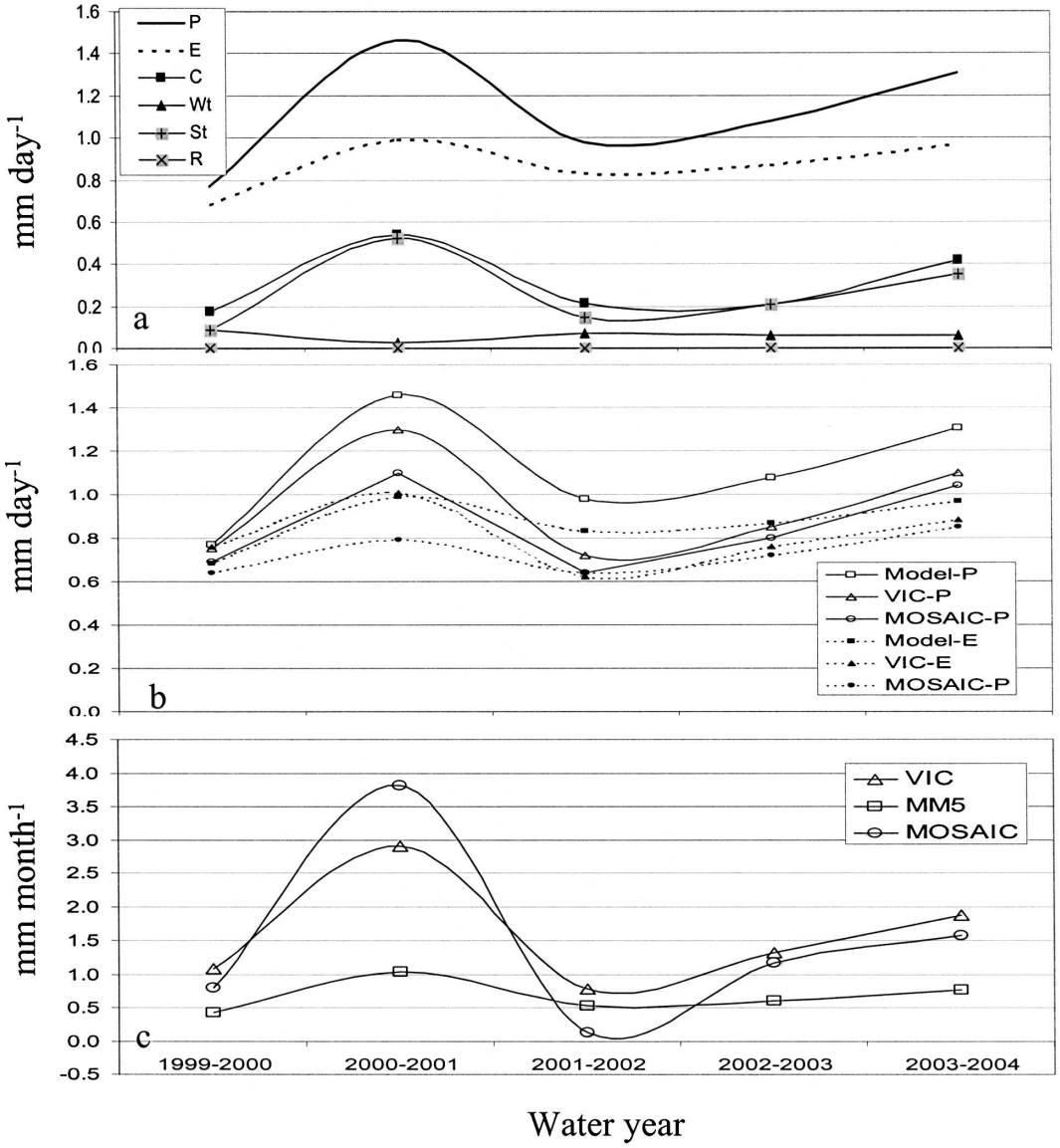

FIG. 8. The interannual variation of the hydrologic component mean over the upper Rio Grande basin for the 5-water-year period. The letters in the figure represent P, precipitation; E, evaporation; C, convergence; W_t, storage time derivative over the atmosphere; S_t, time derivative of land surface storage; and R, grid runoff; (a) from MM5 output, (b) the precipitation and evaporation comparison among the MM5, VIC, and Mosaic model outputs, and (c) surface runoff comparison among MM5, VIC, and Mosaic data.

Figure 8c shows the corresponding mean grid runoff interannual variation over the upper Rio Grande basin. In contrast to evaporation, the interannual variation of Mosaic runoff showed a greater amplification than that of the VIC runoff. Figure 8c indicates that the Mosaic runoff was larger than VIC runoff in a wet year and smaller in a dry year. Although the MM5 shows large runoff differences in comparison with the VIC and Mosaic, the MM5 exhibits similar variation trends as the VIC and Mosaic data. Comparing Figs. 6 and 8 shows that the runoff (the time derivative of land surface storage S_t) from MM5 was smaller (larger) than that from the VIC and Mosaic, which means that in the current model configuration, MM5 allocated more precipitation to the S_t than runoff than the VIC and Mosaic systems did, partly because the MM5 system had a negative soil moisture bias.

Figure 9 compares the interannual variability in precipitation, evaporation, and runoff over the upper Rio Grande basin. In comparison with the VIC and Mosaic systems, MM5 simulated the variability very well in terms of trends but not in terms of amounts. The au-

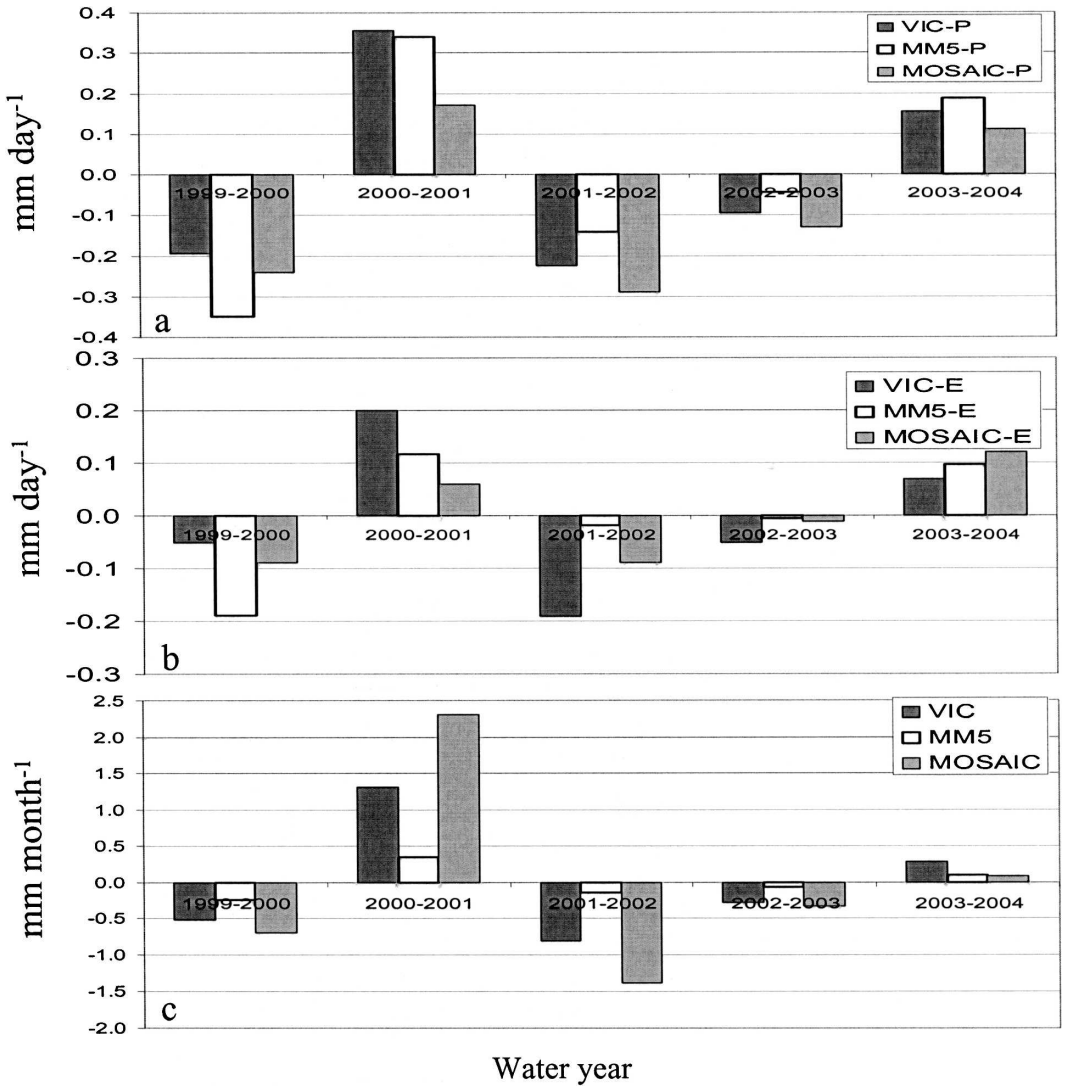

FIG. 9. Interannual variability comparison of (a) precipitation, (b) evaporation, and (c) runoff among MM5, VIC, and Mosaic output over the upper Rio Grande basin for the five-water-year period.

thors also analyzed the variability in the other hydrologic component outputs from the MM5 and found that the variability of convergence, precipitation, and land storage time derivative was highly correlated for the five water years. The variability of W_t is the opposite of runoff, that is, when W_t increases in amount, runoff decreases in value (not shown).

Figure 10 shows the spatial distributions of $E - P$, C, S_t, and R over domain 4 in the wet (2000/01) and dry (2001/02) water years. The distribution of S_t was similar to that of C in both the dry and wet years. These results indicate that, as discussed above, variability in large-scale convergence is the main cause of variability in land surface water storage time derivative. The difference between the wet year and the dry year occurred mainly in central New Mexico, where the signs of $E - P$, C, and S_t had changed. In the dry year of 2001/02, S_t was negative because $E - P$ was greater than zero. This implies that the water mass "diverged" from this area. In contrast, during the wet water year of 2000/01, water mass converged to this area, resulting in positive S_t. The results shown in Fig. 10 indicate that managing water resources is more important and difficult in the above-mentioned areas, where E was usually close to (or greater than) P, than in other places because evaporation will cause these areas to become dry, a condition that is exacerbated because less water is transported here from outside to compensate for this deficit.

Figure 11 compares the time series of daily SWE averaged separately through 22 SNOTEL stations and

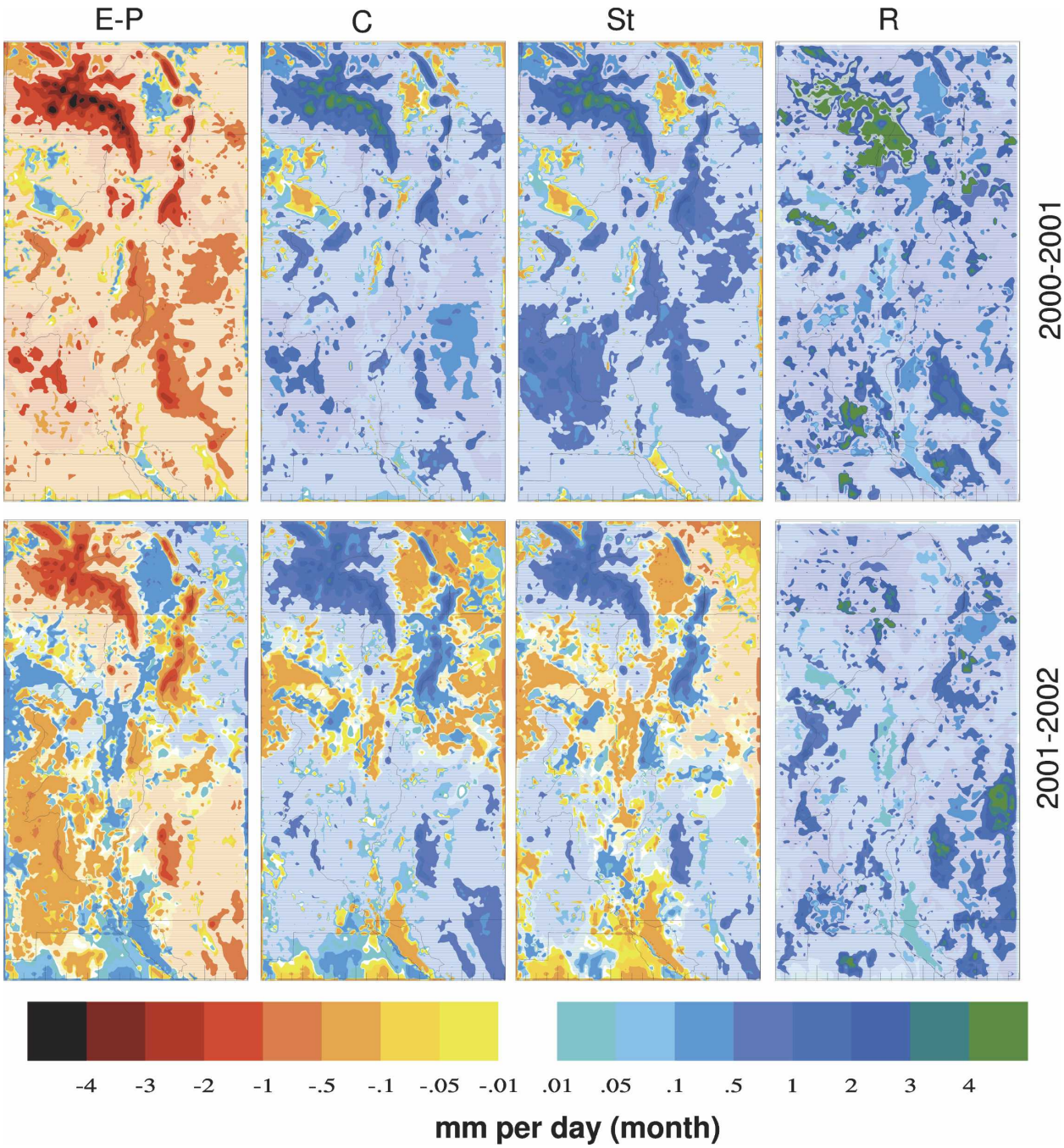

FIG. 10. Maps of $E - P$ (mm day^{-1}), convergence (mm day^{-1}), surface storage time derivative (mm day^{-1}), and monthly grid runoff (mm) in the water years of 2000/01 and 2001/02.

the MM5 4-km grid cells closest to the SNOTEL stations for the 2000/01 and 2001/02 winter seasons. Here, the 2000/01 winter was snow rich, and the 2001/02 winter was snow deficient. The model time series of SWE matched the SNOTEL observation fairly well in the snow-deficient winter of 2001/02 but severely underestimated the snow-rich winter of 2000/01. Figure 5a shows that the model overestimated the winter precipitation for both the snow-deficient and snow-rich winters. Therefore, the MM5–Noah model shows a severe deficiency in that it systematically underestimates the snow cover on the land surface. The Noah land surface model (Chen and Dudhia 2001) simplifies snowpack on the land surface as a single layer of ice particles without

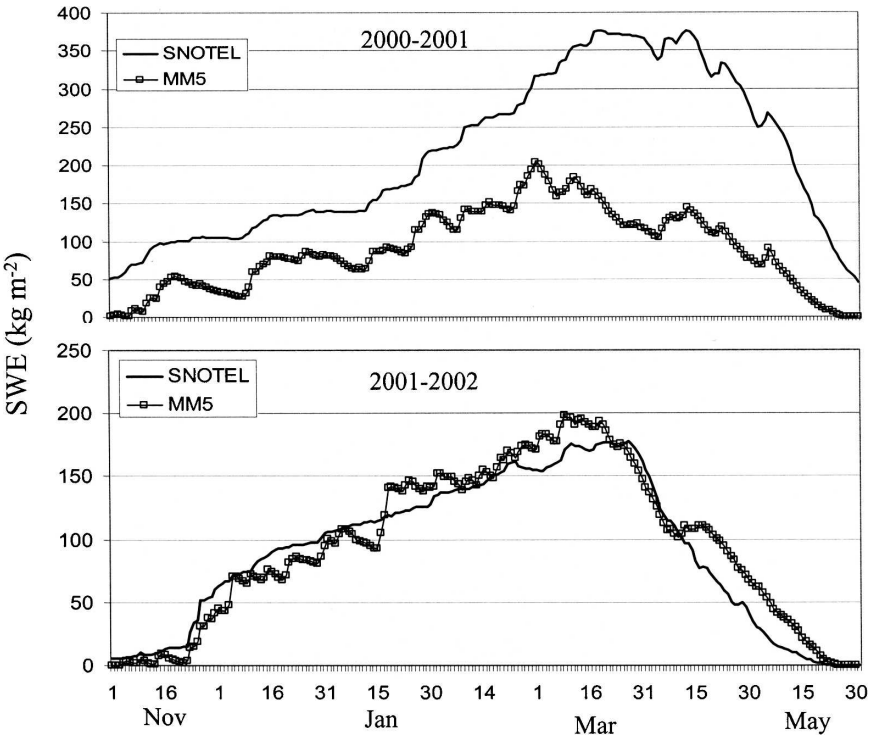

FIG. 11. Mean daily SWE comparison between SNOTEL data and that of the MM5 grid point closest to the SNOTEL station in the winters of 2000/01 and 2001/02. Data from a total of 22 SNOTEL stations were available over the basin during the simulation period.

liquid water. The physical properties of snowpack do not change with snow age and density variation. Many previous studies about physically based snow models (Narapusetty and Molders 2005; Fassnacht et al. 2006; Simpson et al. 2004; Strack et al. 2004) have demonstrated that these simplifications will result in unrealistic snow cover and SWE on the land surface. In addition, model errors in meteorological simulation can affect the simulation of snow processes. Figure 5d shows that the modeled 2-m air temperature in the 2000/01 winter season had a larger positive bias than in the 2001/02 winter season. The warmer air temperature might have resulted in less snowfall and an easy snowmelt. Because snow is the major water source for maintaining river water and groundwater in the semiarid southwestern United States, the model's deficiency in snow simulation will greatly limit its use for water resource applications.

c. Annual variation

Figures 12a–c show the variations in annual mean of precipitation, evaporation, and runoff for the MM5, VIC, and Mosaic data. Figure 12a shows that monthly mean precipitation over the basin exhibits two distinct annual peaks: one in the late winter and early spring that is associated with wintertime frontal precipitation and the other in the late summer and early autumn, which corresponds to the monsoon convective rainfall.

However, in wintertime, MM5 overestimated precipitation, possibly because the continuous 4-month run in the winter seasons occurs without initialization. Qian et al. (2003) tested model performance by reinitializing the regional climate model for every 10, 30, and 90 days and found that the model result is improved when the model is reinitialized every 10 days. We also tested model performance in January 2001 by reinitializing the model run every 4 months (T1), every month (T2), and every 10 days (T3). The mean precipitation over the basin for the test month changed to 75 mm for T1, 63 mm for T2, and 37 mm for T3, in comparison with 41.5 mm for VIC and 27 mm for Mosaic.

Figure 12b compares evaporation from the three models. The differences are apparent. In Mosaic and MM5, evaporation showed two peaks, while evaporation from VIC only had one peak. In comparison with the VIC evaporation, MM5 overestimated evaporation from autumn to early next spring and underestimated it from the late spring to summer.

Figure 12c shows the annual variation of grid runoff

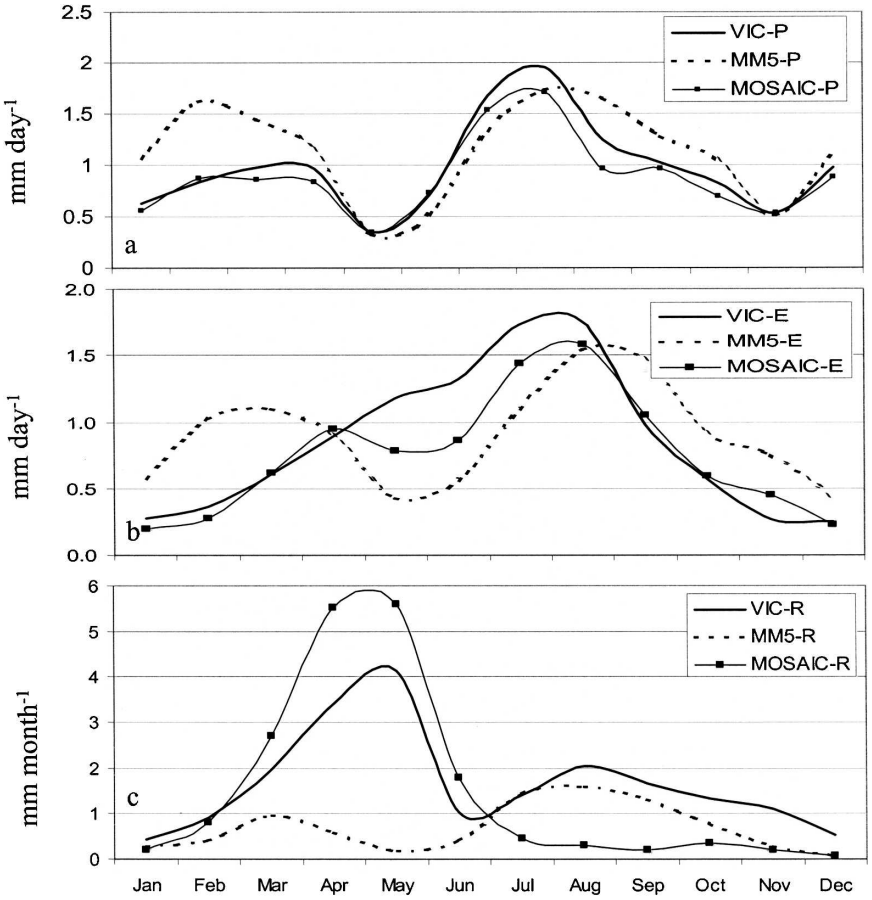

FIG. 12. Intraannual variation of (a) mean precipitation, (b) evaporation, and (c) surface grid runoff for VIC, Mosaic, and MM5 output over the upper Rio Grande basin.

mean in the three models. In comparison with VIC runoff, Mosaic accurately reproduced the runoff that occurred from late winter to spring but amplified and failed to reproduce the runoff that occurred in summer and autumn. MM5 severely underestimated the runoff that occurred in the springtime but fairly accurately generated the runoff that occurred in summer and autumn.

The annual variability in precipitation, evaporation, and runoff from VIC, Mosaic, and MM5 also indicates (not shown) that MM5 fails to accurately reproduce annual variability, especially during the spring season.

Some of the reasons that the model incorrectly simulated evaporation and runoff at an annual scale include the following:

1) The model generated positive biases in predicting the surface air temperature during the winter season (Fig. 5d). The positive bias in the surface temperature accelerated the rate at which precipitation evaporated and/or snowpack melted during winter and springtime. The overestimated evaporation in the winter and springtime caused the model to underestimate the evaporation from April to June.
2) The model generated a negative bias in predicting soil moisture. Figure 3 shows that the modeled soil moisture was relatively low after the 10-day spinup period. The low soil moisture value in the surface soil layer was reflected, on the one hand, in a small amount of evaporation in the dry season, and, on the other hand, in a large land water storage change in the wet season.

Gochis et al. (2003) reported that the Rio Grande acted as a source of moisture in July 1999 when the Grell CPS was used (their Table 1 in which $E - P$ equals 10.6 mm). Our study checked the amount of precipitation and evaporation in July 1999 over the upper Rio Grande and found that precipitation was 41.4 mm month^{-1} and evaporation was 52 mm month^{-1}, a

result that is consistent with that of Gochis et al. The differences in the amounts of $E - P$ between Gochis et al.'s results and those in Fig. 12 are due to the use of a different time period and region.

The results presented in Fig. 12 imply that the MM5 model can reproduce the annual precipitation variation trend. However, the model had a limited ability to reproduce evaporation and runoff and their annual variability in the cold season.

6. Summary

This manuscript reports on research that downscaled 5 yr (i.e., water years 2000–04) of data on the hydrometeorological fields of the upper Rio Grande basin to a 4-km grid using a regional model (MM5, version 3) and the NCEP–NCAR reanalysis data. The available data from observation, analysis, and other models, like VIC and Mosaic, are employed for comparison. The results indicate the following:

1) In general, the hydrologic components, including precipitation, evaporation, and runoff, from three models (MM5, VIC, and Mosaic) show differences in both amount and/or spatial distribution partly because observations were sparse and because the models showed differences in parameters and physics contributions. For example, the 5-yr mean of the water cycle components over the upper Rio Grande basin were as follows from the MM5, VIC, and Mosaic systems, respectively: precipitation was 1.13, 1.01 (NCDC/COOP gauge) and 0.91 mm day^{-1} (NCEP gridded gauge), and evaporation was 0.93, 0.89, and 0.78 mm day^{-1}.
2) The results from the three models indicate that with an increase in elevation, hydrologic components, such as precipitation, evaporation (evapotranspiration), and convergence, show an increasing trend. Also, with an increase in elevation, convergence becomes as important as evaporation in balancing the precipitation in the water cycle, although evaporation dominates in the basin's low-elevation region.
3) The three models' results also indicate similar interannual variability trends in precipitation, evaporation, and runoff, although the amounts from the three models differ.
4) The result from MM5 also shows the following features:
   (i) Compared with previous model studies, which were at a lower resolution, the use of high spatial resolution simulations improved the model's performance in predicting the diurnal cycle.
   (ii) The MM5 can also reproduce the distribution of precipitation features that are caused by terrain, in comparison with observations and especially in comparison with SNOTEL precipitation.
   (iii) The MM5's mean recycling ratio was 0.78, which means that approximately 80% of the precipitation moisture was due to local recycling, while about 20% of the precipitation moisture came from the large-scale convergence. This result is consistent with previous studies in the region, although the recycling ratio was relatively low in comparison with those from VIC and Mosaic.
5) Even though the high-resolution MM5 showed some promising results, it also exhibited some shortcomings. The main deficiencies identified are the following:
   (i) The model cannot reproduce the annual variability of precipitation, evaporation, and runoff, especially for cold seasons. At the annual scale, both the observations and the model results show precipitation as having two distinct peaks. These peaks correspond to the cold season frontal precipitation and the summer monsoon convective storms. However, the model exhibited some inabilities to reproduce precipitation and evaporation annual variability, in comparison with the results extracted from the VIC and Mosaic systems, especially in the cold season.
   (ii) The model has a deficiency in modeling snowpack, especially in snow-rich years, which is surprising considering that MM5 typically overestimates precipitation. This suggests that the model generated evaporation variation and runoff incorrectly in the snow season and the following two months.

The MM5 results in the study region enabled us to identify some special areas, "hydrometeorological hotspots," where evaporation exceeded precipitation and moisture divergence prevailed (Figs. 6 and 10), while the results from VIC and Mosaic indicate that these signals (i.e., $E > P$) are very weak. The MM5's results regarding these hydrometeorological features need further investigation.

Finally, given the importance of snow in this basin, we are currently investigating ways to improve snowpack simulation and study the possible effects of different forcing data on the way the model renders the hydrologic cycle.

Acknowledgments. The reviewers' suggestions and comments were greatly helpful to finalize the manuscript. The authors first thank Dr. Andrew W. Wood at

the University of Washington for providing the offline VIC model output data. The authors also thank Jimmy Ferng and CCIT at the University of Arizona for providing computer resources and assistances. Primary support for this research was provided under the NOAA GAPP Program (NA16GP1605), NASA NEWS/NNG06GB20G, and the NSF-STC Program (Agreement EAR-9876800). The authors thank Ms. Diane Hohnbaum for her help in editing the manuscript.

REFERENCE

Anderson, B. T., and H. Kanamaru, 2005: The diurnal cycle of the summertime atmospheric hydrologic cycle over the southwestern United States. *J. Hydrometeor.,* **6,** 219–228.

——, ——, and J. O. Roads, 2004: The summertime atmospheric hydrologic cycle over the southwestern United States. *J. Hydrometeor.,* **5,** 679–692.

Berbery, E. H., and E. M. Ramusson, 1999: Mississippi moisture budgets on regional scales. *Mon. Wea. Rev.,* **127,** 2654–2673.

Bowen, B. M., 1996: Rainfall and climate variation over a sloping New Mexico plateau during the North American monsoon. *J. Climate,* **9,** 3432–3442.

Chen, F., and J. Dudhia, 2001: Coupling an advanced land surface–hydrology model with the Penn State–NCAR MM5 modeling system. Part I: Model implementation and sensitivity. *Mon. Wea. Rev.,* **129,** 569–585.

Cosgrove, B. A., and Coauthors, 2003: Real-time and retrospective forcing in the North American Land Data Assimilation System (NLDAS) project. *J. Geophys. Res.,* **108,** 8842, doi:10.1029/2002JD003118.

Dudhia, J., 1989: Numerical study of convection observed during the Winter Monsoon Experiment using a mesoscale two-dimensional model. *J. Atmos. Sci.,* **46,** 3077–3107.

Fassnacht, S. R., Z.-L. Yang, K. R. Snelgrove, E. D. Soulis, and N. Kouwen, 2006: Effects of averaging and separating soil moisture and temperature in the presence of snow cover in a SVAT and hydrological model for a southern Ontario, Canada, watershed. *J. Hydrometeor.,* **7,** 298–304.

Giorgi, F., and G. T. Bates, 1989: The climatological skill of a regional model over complex terrain. *Mon. Wea. Rev.,* **117,** 2325–2347.

——, ——, and S. J. Nieman, 1993: The multiyear surface climatology of a regional atmospheric model over the western United States. *J. Climate,* **6,** 75–92.

——, C. S. Brodeur, and G. T. Bates, 1994: Regional climate change scenarios over the United States produced with a nested regional climate model. *J. Climate,* **7,** 375–399.

Gochis, D. J., W. J. Shuttleworth, and Z.-L. Yang, 2003: Hydrological responses of the modeled North American monsoon to convective parameterization. *J. Hydrometeor.,* **4,** 234–250.

Grell, G. A., 1993: Prognostic evaluation of assumptions used by cumulus parameterizations. *Mon. Wea. Rev.,* **121,** 764–787.

Hong, S.-Y., and H.-L. Pan, 1996: Nonlocal boundary layer vertical diffusion in a medium-range forecast model. *Mon. Wea. Rev.,* **124,** 2322–2339.

Kain, J. S., and J. M. Fritsch, 1990: A one-dimensional entraining/detraining plume model and its application in convective parameterization. *J. Atmos. Sci.,* **47,** 2784–2802.

Kanamitsu, M., and K. C. Mo, 2003: Dynamical effect of land surface processes on summer precipitation over the southwestern United States. *J. Climate,* **16,** 496–509.

Kim, J., and J.-J. Lee, 2003: A multiyear regional climate hindcast for the western United States using the mesoscale atmospheric simulation model. *J. Hydrometeor.,* **4,** 878–890.

Leung, L. R., and Y. Qian, 2003: The sensitivity of precipitation and snowpack simulations to model resolution via nesting in regions of complex terrain. *J. Hydrometeor.,* **4,** 1025–1043.

——, ——, and X. Bian, 2003a: Hydroclimate of the western United States based on observations and regional climate simulation of 1981–2000. Part I: Seasonal statistics. *J. Climate,* **16,** 1892–1911.

——, ——, J. Han, and J. O. Roads, 2003b: Intercomparison of global reanalyses and regional simulation of cold season water budgets in the western United States. *J. Hydrometeor.,* **4,** 1067–1087.

Li, J., X. Gao, R. Maddox, and S. Sorooshian, 2005: Sensitivity of North American monsoon rainfall to multisource sea surface temperatures in MM5. *Mon. Wea. Rev.,* **133,** 2922–2939.

Liang, X., L. Li, K. E. Kunkel, M. Ting, and J. X. L. Wang, 2004: Regional climate model simulation of U.S. precipitation during 1982–2002. Part I: Annual cycle. *J. Climate,* **17,** 3510–3529.

Maurer, E. P., A. W. Wood, J. C. Adam, and D. P. Lettenmaier, 2002: A long-term hydrologically based dataset of land surface fluxes and states for the conterminous United States. *J. Climate,* **15,** 3237–3251.

Mitchell, K. E., and Coauthors, 2004: The multi-institution North American Land Data Assimilation system (NLDAS): Utilizing multiple GCIP products and partners in a continental distributed hydrological modeling system. *J. Geophys. Res.,* **109,** D07S90, doi:10.1029/2003JD003823.

Narapusetty, B., and N. Molders, 2005: Evaluation of snow depth and soil temperatures predicted by the Hydro–Thermodynamic Soil–Vegetation Scheme coupled with the fifth-generation Pennsylvania State University–NCAR mesoscale model. *J. Appl. Meteor.,* **44,** 1827–1843.

Qian, J., A. Seth, and S. Zebiak, 2003: Reinitialization versus continuous simulations for regional climate downscaling. *Mon. Wea. Rev.,* **131,** 2857–2874.

Roads, J. O., and S.-C. Chen, 2000: Surface water and energy budgets in the NCEP regional spectral model. *J. Geophys. Res.,* **105,** 29 539–29 550.

——, ——, A. K. Guetter, and K. P. Georgakakos, 1994: Large-scale aspects of the United States hydrologic cycle. *Bull. Amer. Meteor. Soc.,* **75,** 720–734.

Schmitz, J. T., and S. L. Mullen, 1996: Water vapor transport associated with the summertime North American monsoon as depicted by ECMWF analyses. *J. Climate,* **9,** 1621–1634.

Simpson, J. J., M. D. Dettinger, F. Gehrke, T. J. Mcintier, and G. L. Hufford, 2004: Hydrologic scales, cloud variability, remote sensing, and models: Implications for forecasting snowmelt and streamflow. *Wea. Forecasting,* **19,** 251–276.

Small, E., 2001: The influence of soil moisture anomalies on variability of the North American monsoon system. *Geophys. Res. Lett.,* **28,** 139–142.

Strack, J. E., G. E. Liston, and R. A. Pielke Sr., 2004: Modeling snow depth for improved simulation of snow–vegetation–atmosphere interactions. *J. Hydrometeor.,* **5,** 723–734.

Warner, T. T., and H.-M. Hsu, 2000: Nested-model simulation of most convection: The impact of coarse-grid parameterized convection on fine-grid resolved convection. *Mon. Wea. Rev.,* **128,** 2211–2231.

Xu, J., X. Gao, S. Sorooshian, J. Shuttleworth, and E. Small, 2004: Soil moisture–precipitation feedback on the North American monsoon system in the MM5-OSU model. *Quart. J. Roy. Meteor. Soc.,* **130,** 2873–2890.

Zangvil, A., A. H. Portis, and P. J. Lamb, 2004: Investigation of the large-scale atmospheric moisture field over the midwestern United States in relation to summer precipitation. Part II: Recycling of the local evapotranspiration and association soil moisture and crop yields. *J. Climate,* **17,** 3282–3301.